Draft version February 4, 2016
Preprint typeset using LaTeX style emulateapj v. 12/16/11

EFFECT OF MULTIPLE REFLECTION OF THE SKY SIGNAL OFF THE HERA ELEMENT ON THE MEASUREMENTS OF 21CM POWER SPECTRUM

Nipanjana Patra[1], Zaki Ali[1], Carina Cheng[1], Dave DeBoer[1], and Gilbert Hsyu[2], Tsz Kuk Leung[2], Aaron Parsons[1]

Draft version February 4, 2016

ABSTRACT

1. INTRODUCTION

Since it was first proposed in (**?**) measuring 21 cm emission from neutral hydrogen in our early universe has gained attention as a powerful probe of both cosmology and astrophysics. While the science case for 21 cm cosmology, particularly during the Epoch of Reionization, is well established (see, e.g., (Furlanetto et al. 2006; Morales & Wyithe 2010; **?**)), the technical path toward measuring this signal has been more problematic. The weakness of this hyperfine line keeps the 21 cm signal below opacity throughout cosmological history, but it also creates sensitivity and calibration challenges that have yet to be fully solved. With noise temperatures dominated by sky noise (**?**) and foregrounds four to five orders of magnitude brighter than the signal (**?**), sky-averaged 21 cm monopole experiments such as (EDGES; **?**), (BIGHORNS; **?**), (SARAS; **?**), (SCIHI; **?**), (HyPerion; Presley et al. 2015) and 21 cm reionization power spectrum experiments such as the LOw Frequency ARray (LOFAR; **?**), the Murchison Widefield Array (MWA; **?**), the Giant Metre-wave Radio Telescop (GMRT; **?**), the Donald C. Backer Precision Array to Probe the Epoch of Reionization (PAPER; Parsons et al. 2010), the Hydrogen Epoch of Reionization Array (HERA; **?**), and the future Square Kilometre Array (SKA; **?**) must furnish both collecting area and foreground suppression at levels significantly beyond anything previously achieved in radio telescopes operating below 1 GHz.

One of the most problematic effects facing these experiments is instrument chromaticity. The spectral dimension of 21 cm reionization experiments is of vital importance; for line emission, this coordinate translates to a line-of-sight distance that can be used to construct three-dimensional maps (and power spectra) of emission, as well as probe the evolution of 21 cm emission over cosmological timescales. The evolving response of a radio telescope — either a single dish or an interferometer — versus spectral frequency modulates spectrally smooth foregrounds, contaminating spectral modes that might otherwise be used to measure reionization (**?**). Moreover, the chromaticity of a telescope's response scales linearly with diameter, putting the needs of foreground suppression and signal sensitivity in direct tension with one another.

A major step forward for the field of 21 cm cosmology has been the development of a mathematical description of telescope chromaticity, how it varies with element separation (or telescope diameter), and what it implies for distinguishing foreground emission from the cosmological 21 cm signal (**?**). The "wedge", as it is colloquially known, describes a linear relationship between the separation between elements in an interferometric baseline and the maximum line-of-sight Fourier mode[3] that may be occupied by smooth spectrum foreground emission. At low-order $k_\parallel$ modes within the limits of the wedge, foreground contamination may be suppressed through a combination of calibration and model subtraction. However, calibration or modeling errors rapidly re-establish the characteristic wedge pattern. Outside of the wedge, foreground contamination drops rapidly (Pober et al. 2013; **?**), provided that the spectral responses of antenna elements and analog electronics are sufficiently smooth[4]. In promising avoidance-based foreground strategy employed by PAPER (Parsons et al. 2014; **?**), these modes may be targeted as the lowest risk path for contraining 21 cm reionization in the near term.

In this paper, we examine the performance of a new prototype HERA element in the context of this new wedge-based framework. In coordination with **?**, we compare reflectometry measurements with a specification for the spectral performance of an element, given models of the relative brightness of foreground and 21 cm reionization modes in k-space.

The efficacy of the techniques of foreground removal from the measured data critically limits the 21 cm power spectrum measurements. The delay transformation technique of foreground removal, introduced by (**??**) computes the Fourier transform of the visibility measured by an interferometer and produces a spectrum, referred to as delay spectrum hereafter, which is a function of the geometric time delay corresponding to the physical length of the baseline between two antennas. For the visibilities measured over a wide field across wide frequency bandwidth, the delay spectrum is constituted by the instrument response, the foreground signal and 21cm power spectrum, hereafter referred to as EoR signal. The technique exploits the smooth spectral characteristics of the foreground and for a widefield wide bandwidth visibility

Contact author email: nipanjana@berkeley.edu
[1] University of California, Berkeley, nipanjana@berkeley.edu
[2] To be inserted

[3] Assuming a flat sky, and using appropriate cosmological scalars, the spectral axis, ν, and angle on the sky, $\vec{\theta}$, translate to coordinates in a three-dimensional volume at cosmological distances. In describing the spatial power spectrum of emission in this volume $P(\vec{k})$, we use the three-dimensional wave vector $\vec{k} \equiv (k_\parallel, \vec{k}_\perp)$, where $k_\parallel$ is aligned with the spectral axis ν, and $\vec{k}_\perp$ lies in the plane of the sky.

[4] Here, we distinguish the chromaticity of the elements in isolation from the chromaticity inherent to element separation in an interferometric baseline.

measurement by an interferometer with a baseline b, confines the foreground contribution to the computed delay spectrum within the largest possible time delay $\tau = b/c$ corresponding to the given baseline length. Such techniques also assumes a spectrally smooth instrumental response whose contribution to the measured data, much as the contribution of the smooth spectrum foreground, also has an upper bound in the delay space imposed by the largest geometric delay of the given baseline. Beyond this limit, for an ideal system performance, the delay spectrum would be dominated by any wideband signal across the sky with spectral and spatial fluctuation over small scale such as the EoR signal and therefore, could be detectable.

The interaction between the sky signal and instrument response can alter the relative contribution of the foreground, instrument response and the EoR signal at a given delay and thus influence the detectability of the EoR signal. Such interactions may cause the foreground and systematics to spill over at higher delays and thus push the upper limit of the foreground and systematic contaminated delay modes to much higher delays. In this process, the EoR signal over large spatial scale will be lost.

The Hydrogen Epoch of Reionization Array (HERA) is a proposed array consisting of 568 14-m dishes in South Africa which will measure the 21 cm power spectrum between 100 to 200 MHz. In this paper, we investigate the performance of the individual HERA elements and resulting contribution of the instrument response to the delay spectrum. Reflectometry measurements are carried out across wide bandwidth on a prototype HERA element in Green Bank, WV (Figure 1) and the results are interpreted in the light of delay spectrum technique. Section 2 describes the delay spectrum for the ideal and non-ideal performance of a two element interferometer. Reflectometry measurements are described in section 3. Section 4 qualifies the performance of the HERA element as an interferometer for detection of the 21 cm power spectrum.

2. VISIBILITY MEASUREMENTS BY A TWO ELEMENT INTERFEROMETER AND THE DELAY SPECTRUM

Consider a two element interferometer with a baseline $\vec{b}$ and antenna field pattern $A(\hat{\theta},\nu)$. If we denote the electric field sky signal in direction $\hat{\theta}$ by $v_{\rm sky}(\vec{\theta},\nu)$ and the receiver noise of each element as $v_{rec}(\nu)$ then the voltage output of each antenna may be written as,

$$v_1(\hat{\theta},\nu) = a_1(\hat{\theta},\nu)v_{\rm sky}(\hat{\theta},\nu)$$

$$v_2(\hat{\theta},\nu) = a_2(\hat{\theta},\nu)v_{\rm sky}(\hat{\theta},\nu)e^{2\pi i\nu\Delta\tau}$$

where $a_1(\hat{\theta},\nu)$ and $a_2(\hat{\theta},\nu)$ are the electric field response patterns of the two antennas. Hence, the time averaged visibility measured by the interferometer may be written as,

$$V(\vec{b},\nu) = \int v_1(\hat{\theta},\nu)v_2^*(\hat{\theta},\nu)e^{-\frac{2\pi i\nu\vec{b}\cdot\hat{\theta}}{c}}d\Omega \qquad (1)$$

We define antenna cross power pattern as $\hat{\theta},\nu) = a_1(\hat{\theta},\nu)a_2^*(\hat{\theta},\nu)$ and denote the sky intensity as $I_{\rm sky}(\hat{\theta},\nu) = v_{\rm sky}(\hat{\theta},\nu)v_{\rm sky}^*(\hat{\theta},\nu)$. Hence,

$$V(\vec{b},\nu) = \int (\hat{\theta},\nu)I_{\rm sky}(\hat{\theta},\nu)e^{-\frac{2\pi i\nu\vec{b}\cdot\hat{\theta}}{c}}d\Omega \qquad (2)$$

In Parsons et al. (2012a), the Fourier transform of the visibility along the frequency axis was introduced, resulting in the delay spctrum:

$$\tilde{V}(\vec{b},\tau) = \iint (\hat{\theta},\nu)I_{\rm sky}(\hat{\theta},\nu)e^{-\frac{2\pi i\nu\vec{b}\cdot\hat{\theta}}{c}}d\Omega\ e^{+2\pi i\nu\tau}d\nu$$
$$= \int \left[A(\hat{\theta},\tau) * I_{sky}(\hat{\theta},\tau) * \delta(\tau - \frac{\vec{b}\cdot\hat{\theta}}{c})\right] d\Omega \qquad (3)$$

The convolution is carried out along the τ axis which is Fourier conjugate of the frequency ν. In words, the sky delay spectrum from any direction $\hat{\theta}$ is convoluted with the delay spectrum of the instrument and would be located at the delay $\tau = \frac{\vec{b}\cdot\hat{\theta}}{c}$ in the delay domain. The maximum geometric delay possible for a given base line would be $\tau_g = \frac{b}{c}$ for the direction of $\hat{\theta} = 0$ when the phase centre is halfway in between the two antennas. Hence, the sky contribution from any direction would be confined within $-\tau_g < \tau < \tau_g$. Due to chromaticity of the sky signal as well as instrument reponse, the delay spectrum of the sky spills over the delay $\tau > \tau_g$ with decaying amplitude [Ref to the figure Parsons12]. Sky delay spectrum $I_{sky}(\tau)$ is contributed by the foreground $I_{fg}(\tau)$ which is spectrally smooth and the 21 cm power spectrum $I_{21}(\tau)$ which contains spectral signatures. Therefore, in the spill over region ($\tau > \tau_g$), the relative strength of the smooth spectrum foreground with respect to the delay spectrum of the I_{21} reduces and the 21 cm delay spectrum could potentially be detectable.

3. EFFECTS OF MULTIPLE REFLECTIONS ON VISIBILITY AND DELAY SPECTRUM

Response of any radio telescope is chromatic and modulates the true sky signal in the spectral domain. This results in the convolution of the instrument response kernel with the sky signal in the delay domain. This fundamentally limits the detectability of a 21 cm power spectrum. In this section, the effect of reflections on the visibility data and corresponding effect on the delay spectrum is discussed qualitatively.

Plane waves incident on a parabolic dish are focussed at the feed which is kept at the focal plane of the dish. The mismatch between the impedance of free space and the feed and transmission line results in a partial coupling of the sky signal into the feed while the rest is reflected off the feed. The reflected signal illuminates the dish and most of it is reflected back into the space. However, a part of it reflects back and forth several times in between the feed and the vertex of the dish which is shadowed by the feed (dashed blue arrows in Figure 2). Such reflections generate multiple copies of the incident sky signal of reduced strength at various delay and phase and thus produces spurious correlations in the visibilities of interferometric data. In this section we compute the visibility of a two element interferometer accounting for the additional reflections of the sky signal in between the feed and the dish vertex and the corresponding effects on the delay spectrum.

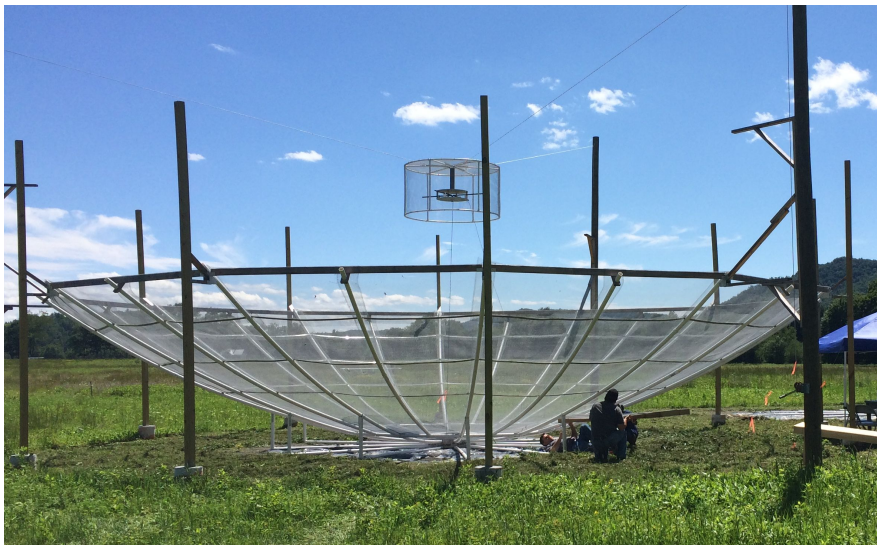

Figure 1. HERA dish and feed at the Green Bank NRAO site.

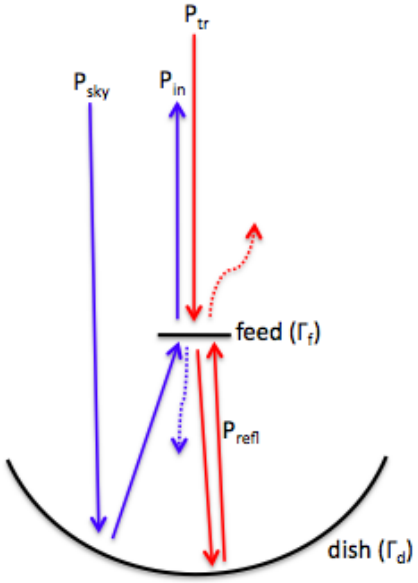

Figure 2. The propagation path of the sky signal entering the feed in receiving mode is shown in blue. Due to impedance mismatch between feed and the free space, a part of the signal (dashed blue) is reflected off the feed. This signal reflects off the dish apex several times and returns to the feed at multiple delays with reduced signal strength. The red line shows the signal path during measurements which is done in transmission mode. Appropriate corrections are made to derive the telescope response function during sky observation.

Consider again a two element interferometer as described in section 2. Two antennas are assumed to be exactly identical so that their electrical parameters and the field pattern are identical i.e, $a_1(\hat{\theta},\nu) = a_2(\hat{\theta},\nu)$. We denote the voltage reflection coefficient of each feed by Γ_f. The voltage reflection coefficient of the reflector dish is denoted by Γ_d. Upon first incidence of the sky signal onto the dish, it is reflected from the entire dish and is focussed onto the feed. Hence, for first incidence $\Gamma_d = 1$. Sky signal that would return to the dish after successive reflections off the feed and the dish is reflected only from a small area around the vertex of the dish and therefore, $\Gamma_d < 1$. In our analysis, we consider one reflection of the sky power from the feed and subsequent reflection off the dish as one single reflection. If the focal length of the dish is l, assuming the feed is located at the focus, the roundtrip delay after first reflection will be $\Delta\tau = \frac{2l}{c}$.

3.1. *Effect of first order reflections on visibility and delay spectrum*

Upon first incidence of the sky signal v_{sky}, Γ_f fraction of the voltage is reflected off the feed while $(1-\Gamma_f)$ fraction is coupled to the feed. The reflected voltage then further reflected off the dish and $(1-\Gamma_f)$ fraction of it reenters the feed with a roundtrip time delay $\Delta\tau$. Hence, the net voltage at the output of the two antennas could be written as,

$$\begin{aligned} v_1 &= a v_{sky}(1-\Gamma_f) + a v_{sky}\Gamma_f\Gamma_d e^{2\pi i\nu\Delta\tau}(1-\Gamma_f)^2 \\ &= a v_{sky}(1-\Gamma_f)\left[1+(1-\Gamma_a)\Gamma_f\Gamma_d e^{2\pi i\nu\Delta\tau}\right] \end{aligned}$$

$$\begin{aligned} v_2 &= \left[a v_{sky}(1-\Gamma_f) + a v_{sky}\Gamma_f\Gamma_d e^{2\pi i\nu\Delta\tau}(1-\Gamma_f)^2\right] e^{\frac{2\pi i\nu\vec{b}\cdot\hat{\theta}}{c}} \\ &= a v_{sky}(1-\Gamma_f)\left[1+(1-\Gamma_a)\Gamma_f\Gamma_d e^{2\pi i\nu\Delta\tau}\right] e^{\frac{2\pi i\nu\vec{b}\cdot\hat{\theta}}{c}} \end{aligned}$$

Frequency as well as angular dependence of the quantities are not written explicitly for notational simplicity. We also absorb the common gain term $(1-\Gamma_f)$ with antenna field pattern a and denote them as $a_f = a(1-\Gamma_f)$ here after and define the antenna cross power pattern as ${}_f(\hat{\theta},\nu) = a_f(\hat{\theta},\nu)a_f^*(\hat{\theta},\nu)$. Hence, the complex visibility could be,

$$\begin{aligned} V(\vec{b},\nu) &= \int v_1 v_2^* d\Omega \\ &= \int_f v_{sky}|^2|\left[1+(1-\Gamma_f)\Gamma_f\Gamma_d e^{2\pi i\nu\Delta\tau}\right]|^2 e^{\frac{2\pi i\nu\vec{b}\cdot\hat{\theta}}{c}} d\Omega \end{aligned} \quad (4)$$

Furthermore, combining all the terms that contain instrument response we define a common instrument pa-

rameter, written as,

$$\Sigma(\vec{b},\nu) = {}_f|\left[1+(1-\Gamma_f)\Gamma_f\Gamma_d e^{2\pi i\nu\Delta\tau}\right]|^2$$
$$= {}_f\left[1+|(1-\Gamma_f)|^2|\Gamma_f|^2|\Gamma_d|^2 + 2\Re\left((1-\Gamma_f)\Gamma_f\Gamma_d e^{2\pi i\nu\Delta\tau}\right)\right] \quad (5)$$

Instrumental response function acquires additional terms arising due to correlation between the directed and reflected component of the sky signal. The total visibility at any frequency would be the sum of the three visibilities contributed by three sources of correlated power. First term in the square bracket represents the cross correlation between the two antenna outputs contributed by the sky signal upon first direct incidence. The second term results from the cross correlation between two reflected signals in each antenna.The last term represents the cross correlation between the first direct incident signal of one antenna and the first reflected signal from the other antenna and vice versa.

Fourier transform of this visibility spectrum along the frequency axis results in the delay spectrum. Fourier transform of the visibility contributed by any two voltage components from two antennas with no mutual delay will be located at the same delay τ in the Fourier domain whereas any two voltage components from two antennas components having a mutual delay of $\Delta\tau$ will be centred at $\tau+\Delta\tau$. This additional delay extends the upper limit on the maximum geometric delay τ_g to $(\tau_g+\Delta\tau)$. Thus, the correlation between the reflected signal from the feed and subsequently from the dish with the direct signal extends the foreground response to delays beyond the maximum geometric delay for a given baseline and contaminates the delay mode where 21 cm delay spectrum could potentially be detected.

3.2. *Effect of multiple reflections on the delay spectrum*

Correlation between the higher order reflections of the signal in any antenna with the direct component of the other would result in a delay response at integral multiple of $\Delta\tau$ and vice versa. If I_{sky} is reflected n times in between the feed and the dish, the net voltage entering the feed after an n^{th} reflection off the feed and the dish is written as:

$$v_1 = a_f v_{sky}[1+(1-\Gamma_f)\Gamma_f\Gamma_d e^{2\pi i\nu\Delta\tau} + (1-\Gamma_f)^2(\Gamma_f\Gamma_d)^2(e^{2\pi i\nu\Delta\tau})^2$$
$$.... + (1-\Gamma_f)^n(\Gamma_f\Gamma_d)^n(e^{2\pi i\nu\Delta\tau})^n]$$

and,

$$v_2 = a_f v_{sky}[1+(1-\Gamma_f)\Gamma_f\Gamma_d e^{2\pi i\nu\Delta\tau} + (1-\Gamma_f)^2(\Gamma_f\Gamma_d)^2(e^{2\pi i\nu\Delta\tau})^2$$
$$.... + (1-\Gamma_f)^n(\Gamma_f\Gamma_d)^n(e^{2\pi i\nu\Delta\tau})^n] * e^{\frac{2\pi i\nu\vec{b}\cdot\hat{\theta}}{c}}$$

The relevant terms in the corresponding visibility and subsequently in the delay spectrum would be the ones which represent the correlation between the direct component of one antenna with the reflected components of the other resulting in higher order terms in $\Sigma(\vec{b},\nu)$. The corresponding instrument response may be written as,

$$\Sigma(\vec{b},\nu) = a_f[1+2\Re[(1-\Gamma_f)\Gamma_f\Gamma_d e^{2\pi i\nu\Delta\tau} + (1-\Gamma_f)^2(\Gamma_f\Gamma_d)^2(e^{2\pi i\nu\Delta}$$
$$.... + (1-\Gamma_f)^n(\Gamma_f\Gamma_d)^n(e^{2\pi i\nu\Delta\tau})^n]]$$
$$= \frac{a_f}{\Gamma_f}\sum_{n=1}^{n}[\Gamma_f\Gamma_d e^{i\phi}]^n$$

and the measured visibility spectrum would be,

$$V(\vec{b},\nu) = \int I_{sky}(\vec{b},\nu)\Sigma(\vec{b},\nu)e^{\frac{2\pi i\nu\vec{b}\cdot\hat{\theta}}{c}}d\Omega \quad (8)$$

Taking the Fourier transform of the visibility we obtain the delay spectrum

$$\tilde{V}(\vec{b},\tau) = \int\left[\int I_{sky}(\vec{b},\nu)\Sigma(\vec{b},\nu)e^{\frac{2\pi i\nu\vec{b}\cdot\hat{\theta}}{c}}d\Omega\right]e^{-2\pi i\nu\tau}d\nu$$
$$= \int\left[I_{sky}(\hat{\theta},\nu) * \Sigma(\hat{\theta},\nu) * \delta(\tau-\frac{\vec{b}\cdot\hat{\theta}}{c})\right]d\Omega \quad (9)$$

The design specification of HERA elements requires that any signal, arriving at the feed at a delay $\Delta\tau$ with respect to the direct incidence, should be at the level of $-60dB$ at a delay of $60ns$ relative to the first incident signal at the feed (Parsons & DeBoer 2015). This specification was approximated based on the power level of the cosmological signal in relation to foreground signals, which is estimated to be six orders of magnitude fainter (Santos et al. 2005; Ali et al. 2008; de Oliveira-Costa et al. 2008; Jelić et al. 2008; Bernardi et al. 2009, 2010; Ghosh et al. 2011). Additionally, the $14m$ HERA baselines set a foreground containing horizon-limit (the wedge) that, with some buffer, sets a delay specification of $60ns$ (Parsons et al. 2012b; Vedantham et al. 2012; Thyagarajan et al. 2013; Liu et al. 2014a,b). Our goal is to determine the effect of the instrument response $\Sigma(\nu)$ on the delay spectrum measurement.

4. MEASUREMENTS

We carried out reflectometry measurements at the HERA element prototype in Green Bank, WV (Figure 1) in order to measure the instrument response of the feed and dish assembly and characterise its performance. An HERA element consists off a $14\,m$ diameter parabolic reflector and a crossed-dipole pair as a feed. The cross dipole antenna pair is identical to the feed of the PAPER antenna which is suspended at the focal plane of the dish with the support of three vertical poles. HERA elements are closely spaced with centre to centre distance between two dishes are equal to the dish diameter. Therefore, to reduce the coupling between the adjacent dishes, the crossed dipole feed along with the back plane is encased in a cylindrical cage. The feed is raised and lowered by a three-pulley system mounted on the three poles. The focal height of the dish is $4.5m$ (~ 14.76ft).

As given in the previous section, if the incident power from the sky signal is I_{sky}, the feed reflection coefficient is Γ_f, and the dish reflection coefficient is Γ_d, then the net power entering a feed after n^{th} reflection off the feed and the dish is:

$$\tilde{I}_{meas}(\vec{b},\nu) = \int I_{sky}(\vec{b},\nu)\Sigma(\vec{b},\nu)e^{\frac{2\pi i\nu\vec{b}\cdot\hat{\theta}}{c}}d\Omega \quad (10)$$

where, $\Delta\tau$ is the roundtrip propagation delay of a frequency ν due to a reflection over the focal distance l. I_{meas} is the auto correlated power obtained from a single HERA element. Upon our assumption that two adjacent antenna elements have identical electrical properties, this power is also a measure of the cross power or the visibility $V(\vec{b},\nu)$ between the two antennas with a normalisation factor of 2. Once again, it is to be noted that upon the first incidence, the sky signal is focussed onto the feed from the entire dish and the dish reflection coefficient Γ_d is 1 for this first incidence. The subsequent back and forth reflection of the signal in between the feed and the dish, however, occurs from only the part of the dish which is shadowed by the feed. Therefore, in this case, $\Gamma_d < 1$. For a given baseline $\vec{b}$, taking the ratio of the measured power and the incident power,

$$\begin{aligned}\frac{I_{meas}}{I_{sky}} &= \Sigma(\vec{b},\nu) \\ &= \frac{a_f}{\Gamma_f}\sum_{n=1}^{n}[\Gamma_f\Gamma_d e^{i\phi}]^n\end{aligned} \quad (11)$$

The right hand side of this equation is the instrument response kernel of a single HERA element as well as a representative of the instrument response in the measured visibility data between a pair of antennas. Our goal is to measure this kernel as a function of frequency and determine its effect on the delay spectrum of the visibility.

4.1. *Method*

The instrument response kernel is measured by measuring the return loss of the antenna element at the output port of the feed using a vector network analyser. The vector network analyser transmits a broadband noise of known amplitude and phase via a $75ft$ cable up to the feed. While a part of this signal is returns to the VNA post reflection from the feed due to mismatch between the cable and the antenna impedance resulting in the primary return loss, rest of the signal is radiated out by the antenna and illuminates the dish and radiated into the space. However, the reflected signal from the dish vertex returns to the feed. This incident signal is now reflected back and forth in between the feed and the dish much like the sky signal reflection discussed previously.

If I_{tr} is the signal transmitted by the VNA , Γ_f is the feed reflection coefficient, I_r is the power incident back on the feed after reflection from the dish then the reflected power, I_{refl}, back into the VNA would be:

$$I_{refl} = I_r A_f[1+\Gamma_f\Gamma_d e^{i\phi}+(\Gamma_f\Gamma_d)^2 e^{i2\phi}+....+(\Gamma_f\Gamma_d)^n e^{in\phi}] \quad (12)$$

Once again, we consider one reflection from the feed and its subsequent reflection from the dish as one reflection in total. Equation 12 is similar to Equation 8, with different incident powers.

I_r is the power that is incident back on the feed, which is just the feed radiated power reflected off the dish:

$$I_r = \Gamma_d(1-\Gamma_f)e^{i\phi}I_{tr} \quad (13)$$

Hence the total returned power P_{ret}, to the VNA would be:

$$\begin{aligned}I_{ret} &= \Gamma_f I_{tr} \\ &+ \Gamma_d(1-\Gamma_f)e^{i\phi}I_{tr}(1-\Gamma_f)[1+\Gamma_f\Gamma_d e^{i\phi}+....+(\Gamma_f\Gamma_d)^n e^{in\phi}]\end{aligned} \quad (14)$$

Simplifying:

$$\begin{aligned}\frac{I_{ret}}{I_{tr}} &= \Gamma_f + \Gamma_d(1-\Gamma_f)^2[e^{i\phi}+\Gamma_f\Gamma_d e^{i2\phi}+....+(\Gamma_f\Gamma_d)^n e^{in\phi}] \\ &= \Gamma_f + \frac{(1-\Gamma_f)a_f}{\Gamma_f}\sum_{n=1}^{n}[\Gamma_f\Gamma_d e^{i\phi}]^n\end{aligned} \quad (15)$$

The ratio in Equation 15 is the returned power to the VNA with respect to the transmitted power sent by the VNA. It is identical to the sky observation case in Equation 11 but differs by two factors. The first factor corresponds to an additive amplitude difference arising from Γ_f, which physically accounts for the initial reflection at the feed. The second difference is a multiplicative term which informs us about the first reflection. Both of these terms need to be corrected for in order to relate our measurements to real observations.

The VNA measures the magnitude and phase of the quantity $\frac{I_{ret}}{I_{tr}}$ as a function of frequency as shown in Figure 3. The magnitude and phase of the complex return loss is measured between 50 to 500MHz over 1024 frequency channels which gives a frequency resolution of 0.44MHz. The delay resolution of the measurements is ?t = 2.22ns. In our measurement set-up, the first reflection occurs at the feed Γ_f, so $(\frac{I_{ret}}{I_{tr}}-\Gamma_f)$ gives an estimate of the delay spectrum of the sky signal. In delay domain, the relative signal strength at zero delay represents the factor Γ_f while the signal strength at any other delay represents any delayed signal that enters the feed after being reflected from the feed surroundings.

4.2. *Estimation of the delay spectrum of the instrument*

Frequency domain data, as shown in Figure 4, is Fourier-transformed to compute the response of the system in the delay domain. The signal transmitted by the VNA is reflected first from the feed. In delay domain, this appears at the zero delay bin. We subtract this value from the measured data and divide the the data by a factor $(1-\Gamma_a)$ to derive the delay spectrum for the system operating in receiving mode during sky observation.

As mentioned in Section **??**, there is a mismatch in amplitude between the reflections that we measure (originating from the FieldFox pulse) and reflections produced by sky signal. The reflections that we measure (at high delays) must be lowered by a factor to represent weaker reflections that would occur after most of the sky signal is received by the feed. For our compensation, we multiply our entire delay spectrum by its DC component, which is the feed reflection coefficient Γ_f, and also divide by $(1-\Gamma_f)$. In other words, these correction factors

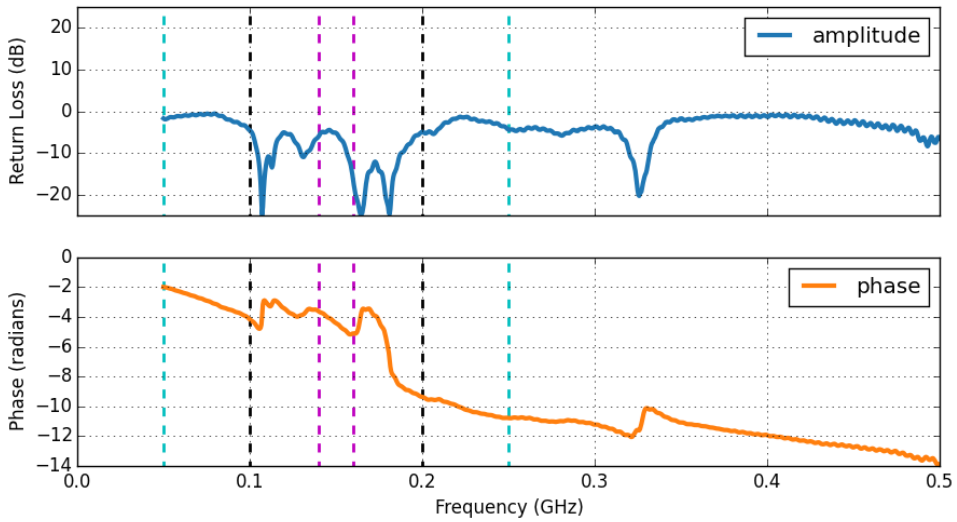

Figure 3. Amplitude and phase of the measured return loss. Colored dashed lines mark three different frequency bands: $140-160MHz$ (typical power spectrum bandwidth), $100-200MHz$ (PAPER bandwidth), and $50-250MHz$ (HERA bandwidth).

equate Equation 15 with Equation 11. We note that this correction is only accurate at high delays where our reflections of interest occur. At low delays, our spectrum amplitude should be increased to represent the original sky signal, but we do not apply this correction because it is not relevant to our analysis.

5. RESULTS

Figure 3 shows the return loss for a frequency bandwidth of 50 to $500MHz$, measured when the feed is suspended at the focal plane of the parabolic dish which is at $4.26m$ from the dish vertex. This measurement is Fourier transformed to obtain the delay spectrum of the instrument in the receiving mode as given in equation 3.

The delay response of the instrument is dependent on the band chosen for the Fourier transform. The measurement bandwidth effects the amplitude and phase of the delay spectrum. Fourier transforms taken over wider bandwidth become dominated by the feed sidelobes outside the operating band, making the resultant delay profiles less relevant for the power spectrum performance of the HERA instrument. Conversely, when performing Fourier transforms over much narrow bands (the windowed $20MHz$ bands typical of PAPER analysis), the width of the resulting delay profile becomes dominated by sidelobes of low delay emission interacting with the narrow bandwidth kernel. Although this may appear to be a relevant performance metric for PAPER power spectrum analysis, such an analysis typically pre-filters out low-delay emission using wide bandwidths precisely to avoid sidelobes from low-delay emission. Hence, the most relevant delay-spectrum performance profile is that taken using the $100-200MHz$ band. **In the $100-200MHz$ delay profile, we see a delay response of $-25dB$ at $60ns$, which slopes down to $-60dB$ at $\sim 120ns$. WRITE AGAIN**

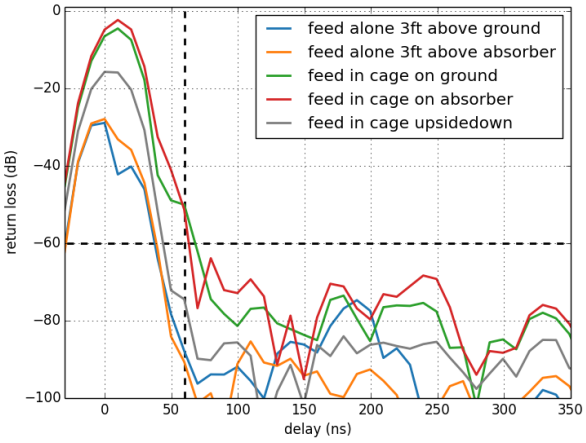

Figure 7. Delay plots produced using a Hamming window function for different feed only configurations and the PAPER bandwidth ($100MHz-200MHz$). The black dashed lines illustrate our "60 by 60" specification.

Figure 6 is again a delay plot of the return loss at four different feed suspension heights. We use the PAPER bandwidth and note that the measurements are near identical at low delays, implying that low delay reflections are caused primarily by reflections within the feed cage. However, at higher delays we notice discrepancies between the different heights. In addition, Figure 5 presents measurements taken of the feed only.away from the dish. Echosorb is placed under the feed for some of the measurements, with the expectation that it will prevent any reflections off the ground. Measurements are also taken of the feed inside its metal cage in various configurations. It is shown that the feed performs best without the cage and with the absorber. All these measurements are suggestive of the fact that the feed-cage assembly itself is responsible for a significant portion of the structure up to $60ns$ and that the cylindrical cage may be contributing up to $20ns$ to the width of the delay profile. We note that this depends stronglyon its coupling to structures around it. Structure beyond $60ns$

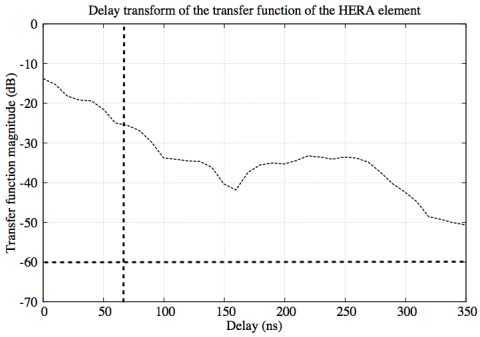

Figure 4. Delay transform of the transfer function of the HERA element. The complex return loss of the element is measured between 50 to 400 MHz when the feed is kept at the focal plane of the dish at a focal height 4.5m. The delay spectrum is produced by taking the Fourier transform of the magnitude of the return loss measurement after limiting the measurements between 100 to 200 MHzusing Blackman-Harris window. The intersection of the horizontal and vertical dashed line shows the instrument performance specification as predicted by the theory of delay transform in order to detect the 21cm power spectrum.

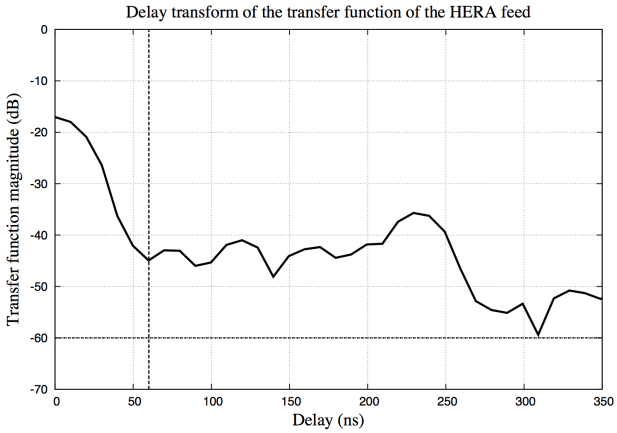

Figure 5. Delay transform of the transfer function of the HERA feed element. The feed is kept on the ground downside up so that the entire radiation from the feed is radiated out. Once again, the measurement is done between 50 to 450 MHz and the delay spectrum is produced between $100 - 200$ MHz by using a Blackman-Harris window. The black dashed lines illustrate the instrument specification.

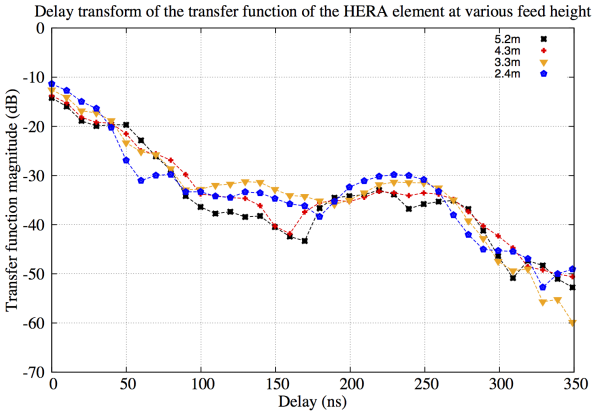

Figure 6. Delay transform of the transfer function of the HERA element keeping the feed at various heights. Delay transform is produced by taking the Fourier transform of the measurement using Blackman-Harris window.

appears to scale with the height of the feed above the dish.

6. CONCLUSION

The delay-domain performance of the HERA dish is central to HERA's function as a power spectrum instrument. As we have seen, reflectometry measurements can help characterize HERA's performance in this domain, and as Equation 11 shows, these measurements must be adjusted for a difference in transmission/reflection at the first feed encounter in order to be interpreted as the delay response of a feed relative to an incident plane wave from the sky. We also see that the choice of windowing function is critical for accurately measuring the antenna delay response at higher delays, where sidelobes from much higher amplitude responses at small delays can easily dominate. We find Hamming, Hanning, and Blackman-Harris windows to be generally adequate while square windowing functions are not. Given the critical nature of the windowing function, we recommend that all reflectometry measurements be performed in the frequency domain, so that the data could be Fourier transformed with the appropriate window.

Taken all together, we summarize that the first version of the HERA dish, with a PAPER-style feed and cylindrical cage, is close to meeting specification, but will require additional work to fall below $-60dB$ at $60ns$. Given that the width of the delay response is a convolution of the feed response and the dish reflections, it is not possible to perfectly decouple the response of the feed from that of the dish. It may be possible to achieve enough of a reduction to meet specification by modifying the feed. Given that previous measurements using a PAPER feed with a simple backplane exhibit structure above $-60dB$ at $60ns$, we deduce that these advances will most likely require improving the feed return loss. We also recommend re-investigating the scattering cone for reducing standing waves between the feed and dish. Finally, given the proximity of our measurements to the rough specification that was adopted for HERA of $-60dB$ attenuation at $60ns$, we recommend reinvestigating this specification to determine more accurately the impact of the element's current delay performance on HERA science. We suspect that, at the level of $-50dB$ at $60ns$ and $-60dB$ at $120ns$, this performance may indeed be adequate for the delay-domain power spectrum analysis for which HERA has been optimized.

REFERENCES

Ali, S. S., Bharadwaj, S., & Chengalur, J. N. 2008, MNRAS, 385, 2166

Bernardi, G., de Bruyn, A. G., Brentjens, M. A., et al. 2009, A&A, 500, 965
Bernardi, G., de Bruyn, A. G., Harker, G., et al. 2010, A&A, 522, A67+
de Oliveira-Costa, A., Tegmark, M., Gaensler, B. M., et al. 2008, MNRAS, 388, 247
Furlanetto, S. R., Oh, S. P., & Briggs, F. H. 2006, Phys. Rep., 433, 181
Ghosh, A., Bharadwaj, S., Ali, S. S., & Chengalur, J. N. 2011, MNRAS, 418, 2584
Jelić, V., Zaroubi, S., Labropoulos, P., et al. 2008, MNRAS, 389, 1319
Liu, A., Parsons, A. R., & Trott, C. M. 2014a, Phys. Rev. D, 90, 023018
—. 2014b, Phys. Rev. D, 90, 023019
Morales, M. F., & Wyithe, J. S. B. 2010, ARA&A, 48, 127
Parsons, A., Pober, J., McQuinn, M., Jacobs, D., & Aguirre, J. 2012a, ApJ, 753, 81
Parsons, A. R., & DeBoer, D. D. 2015
Parsons, A. R., Pober, J. C., Aguirre, J. E., et al. 2012b, ApJ, 756, 165
Parsons, A. R., Backer, D. C., Foster, G. S., et al. 2010, AJ, 139, 1468
Parsons, A. R., Liu, A., Aguirre, J. E., et al. 2014, ApJ, 788, 106
Pober, J. C., Parsons, A. R., Aguirre, J. E., et al. 2013, ApJ, 768, L36
Presley, M., Liu, A., & Parsons, A. 2015, ArXiv e-prints: 1501.01633, arXiv:1501.01633
Santos, M. G., Cooray, A., & Knox, L. 2005, ApJ, 625, 575
Thyagarajan, N., Udaya Shankar, N., Subrahmanyan, R., et al. 2013, ApJ, 776, 6
Vedantham, H., Udaya Shankar, N., & Subrahmanyan, R. 2012, ApJ, 745, 176